Intermolecular Forces and Bond Length Changes in High-Pressure Fluids. Vibrational Spectroscopic Measurement and Generalized Perturbed Hard Fluid Analysis

Yanira Meléndez-Pagán and Dor Ben-Amotz*

Purdue University, Department of Chemistry, West Lafayette, Indiana 47907

Received: May 2, 2000; In Final Form: June 7, 2000

Pressure-dependent vibrational frequency shifts are used to measure intermolecular-interaction-induced forces and bond length changes in solution. The results are employed to quantitate changes in solute−solvent coupling as a function of solvent density using a generalized perturbed hard fluid (G-PHF) analysis of solvent mean-force-induced perturbations of molecular potential energy surfaces. Repulsive solvation forces are calculated using the cavity distribution function of a reference hard-sphere fluid. Attractive forces are treated using a generalized van der Waals mean-field approximation, which allows for both long-range and short-range solute−solvent cohesive interactions. The results indicate marked differences in the density dependence of the attractive solvation force along different types of bonds. Hydrogen stretch vibrations (i.e., C−H and O−H stretches) display a strongly nonlinear density dependence, which is indicative of a short-range attractive solute−solvent coupling mechanism and, thus, is consistent with enhanced C−H and O−H hydrogen-bond formation at high pressure (even in nonpolar solvents). Systems studied include *n*-butanol, acetone, chloroform-*d*, ethane, and methyl iodide in the pure liquid state or dissolved in carbon disulfide, *n*-propyl bromide, *n*-propyl iodide, toluene, 2,3-dimethylbutane, methanol, tetrahydrofuran, or methylene chloride.

I. Introduction

Intermolecular interactions hold the key to understanding the structural, spectroscopic, and chemical properties of condensed-phase materials. This work is aimed at quantifying such interactions by measuring the changes in the vibrational frequencies of solute molecules in liquids as a function of pressure. The resulting frequency shift measurements are analyzed using a generalized (G) form of the perturbed hard fluid (PHF) model.[1−6] This G-PHF model extends the PHF model by including the influence of both short- and long-range cohesive solute−solvent coupling mechanisms. The results indicate that the attractive force length scale can be quantitatively determined using density-dependent (pressure-dependent) experimental measurements and, thus, that the unique vibrational frequency shift behavior of C−H and O−H vibrations[7,8] is consistent with the enhanced formation of short-range solute−solvent hydrogen bonds at high pressures, even in nonpolar solvents.

When a molecule is transferred from the gas to the liquid phase, it may undergo a shift in vibrational frequency, $\Delta\nu_{g-l}$, and a change in bond lengths, Δr_{g-l}, in response to the mean force, F_{g-l}, produced by solute−solvent interactions.[9] Both $\Delta\nu_{g-l}$ and F_{g-l}, are typically negative in low-pressure vapor and fluid phases and positive in high-pressure fluids (and solids), while Δr_{g-l} has the opposite sign. In other words, a negative mean force produces a decrease in vibrational frequency (red shift) and an elongation of the corresponding bond, because of preferential solvation of the excited vibrational state (and conversely for a blue shift). Thus, *pressure-induced vibrational frequency shifts can be used to probe the delicate balance and competition between attractive and repulsive solute−solvent coupling mechanisms*.[4]

In this work, Raman spectroscopic frequency shifts are used to measure pressure-induced solvation forces and bond length changes in chloroform-*d* (C−D stretch and C−Cl stretch) and acetone (C−C stretch) dissolved in various solvents (methanol, dichloromethane, and tetrahydrofuran). These are combined with previously reported infrared shifts of the O−H stretch in dilute *n*-butanol solutions[10] and Raman shifts in fluid nitrogen, ethane, and methyl iodide[8] at pressures up to 2.5 GPa. The results are used to quantify the solvent mean force and bond length changes of different solute vibrational modes, with a sensitivity of about ±8 picoNewtons (pN) in F_{g-l} and ±0.005 Å in Δr_{g-l}.

Vibrations involving hydrogen or deuterium atoms (i.e., C−H, C−D, O−H, or O−D) are of particular interest, as they have long been known to shift in an unusual way with solvent density.[1,5,7−9] Specifically, at liquid densities, nonhydrogen vibrations invariably shift to higher frequencies, producing a nonlinear density dependence with positive curvature. Hydrogen vibrations, on the other hand, often appear to shift downward nonlinearly (with negative curvature) at moderate densities, before beginning to shift upward (with positive curvature) at high densities.[1,7,8] The most extreme behavior is observed for alcohols dissolved in a variety of both polar and nonpolar solvents. The solute O−H stretch vibrations in these systems continue to red shift in a strongly nonlinear way at pressures up to 1 GPa (∼10 000 atm),[10] long after all other vibrations have succumbed to compressive forces by blue shifting.[1,8,9]

The unique behavior of hydrogen vibrations has been quantified in several previous studies as a deviation from the predictions of perturbative models,[1,4,5,7,8] which predict a linear attractive-force-induced red shift at low density and a nonlinear repulsive-force-induced blue shift with *positive curvature* at high densities. The nonlinear red shifts of hydrogen vibrations (with *negative curvature*) in high-pressure solutions have been phenomenologically fit to a quadratic density dependence.[7,10] However, C−H, H_2, and HCl frequency shift studies in supercritical fluids[8,11−14] reveal a clearly linear (rather than quadratic) hydrogen red shift up to near critical densities. Such

10.1021/jp0016479 CCC: $19.00
Published on Web 07/26/2000

linear behavior at low-to-moderate densities is consistent with fundamental theoretical predictions[4,5,15−19] (and is also typical of that observed for nonhydrogen vibrations.[8,11,20] Thus, the red shift of hydrogen vibrations is clearly not a quadratic function of density over the entire gas-to-liquid density range.

Intramolecular Fermi resonance or intermolecular resonance couplings have been suggested as possible mechanisms for the unusual behavior of hydrogen vibrations.[8] However, these mechanisms do not appear to be compatible with available data, including quantitative C−H Fermi resonance-corrected measurements[8,21] and O−H frequency shift studies in dilute solutions lacking intermolecular resonance (such as butanol in CS_2).[7,10] The present studies of dilute chloroform-*d* dissolved in nondeuterated solvents further undermine any such resonance-coupling-based explanations, as these systems lack intra- or intermolecular vibrational resonances anywhere near the solute C−D stretch frequency.

The explanation that emerges from the present work builds on a suggestion made by Zakin and Herschbach, who proposed solvent packing effects as a possible mechanism for the nonlinear density dependence of hydrogen vibrational shifts. Zakin and Herschbach's calculations for a model fluid composed of spherical Lennard-Jones particles confirmed that attractive interactions that scale as $-(C/r^6)$ could indeed produce a nonlinear density-dependent frequency shift of negative curvature. However, the magnitude of the predicted curvature was significantly smaller than that required to quantitatively reproduce experimental hydrogen frequency shifts.[7] The present G-PHF analysis expands on Zakin and Herschbach's suggestion by demonstrating that more strongly nonlinear attractive-force-induced frequency shifts are consistent with the influence of packing effects in a system with cohesive interaction of significantly shorter range than $-(C/r^6)$. Thus, hydrogen bonding (or some other short-range solute−solvent cohesive interaction) is suggested as the most viable explanation for the anomalous frequency shift behavior of hydrogen vibrations.

The remainder of this paper is organized as follows. Section II describes the theoretical expressions used to extract molecular forces and bond length changes from vibrational frequency shifts. Section III (and the Appendix) describes the G-PHF model used to interpret gas-to-liquid and pressure-induced frequency shifts of both hydrogen and nonhydrogen vibrations. Section IV describes the experimental method used to measure pressure-induced Raman scattering frequency shifts. Section V summarizes the results and global trends revealed in comparing force and bond length measurements in different systems. Section VI summarizes the results and conclusions of this work.

II. Molecular Force and Bond Length Measurement

The theoretical relationship between vibrational frequency shifts and intermolecular forces has been discussed in detail previously.[9,15] Briefly, a general expression derived by David Buckingham,[22,23] when truncated to first order in the solvent configuration-averaged mean force, F, along the solute bond, reduces to the following approximate expression for the vibrational frequency shift, $\Delta\nu$, of the corresponding solute bond.

$$\Delta\nu \approx -\frac{3}{2}\frac{\nu_e g}{f^2}\langle U'\rangle \tag{1}$$

Inverting the above equation yields an expression relating the force along the bond and its change in bond length, Δr, to a product of experimentally measurable parameters.

$$\langle U'\rangle \equiv F \approx \left[\frac{-2f^2}{3\nu^e g}\right]\Delta\nu \tag{2}$$

$$\Delta r = -F/f \tag{3}$$

where f and g are the harmonic and anharmonic force constants of the isolated solute, respectively, and ν_e is the classical harmonic frequency. Although the above expressions leave out the next higher term (related to the solvent force fluctuations[1,15,24]), eqs 2 and 3 are believed to have an absolute quantitative accuracy of ±50% and presumably are even more accurate in describing relative changes in F and Δr (as a function of solvent density and in comparisons of results for a series of different solvents).[9] In addition, although the above expressions are derived for a diatomic solute, they have been applied to polyatomic normal modes using a pseudodiatomic approximation.[1,5,8,25] Alternative approximate treatments of polyatomic vibrations have modeled polyatomic vibrations as a superposition of local diatomic bond vibrations[4] or by using a spherically averaged potential with normal-mode-coordinate-dependent parameters.[16,26] All of these approaches involve a substantial degree of approximation and are not believed to be significantly more accurate than the pseudodiatomic approximation used in this work (although there is certainly room for debate, and further work, in this area).

Note that the frequency shift, $\Delta\nu$, appearing in eq 2 represents the change in frequency observed when a molecule is transferred from one thermodynamic system to another. Thus, $\Delta\nu$ could be a gas-to-liquid shift or a shift observed in transferring a solute from one solvent to another or in going from an ambient liquid to the same liquid at high pressure. The particular reference state chosen in defining $\Delta\nu$ determines the reference with respect to which F and Δr are determined. Thus, if $\Delta\nu = \Delta\nu_{g-l}$, then $F = F_{g-l}$ and $\Delta r = \Delta r_{g-l}$ represent the total solvation-induced force and bond length change, respectively, relative to an ideal gas reference state. In general, however, $\Delta\nu$, F, and Δr, may represent relative changes with respect to any other specified reference state. In either case, the constants f, g, and ν_e can be taken to be those of the isolated solute molecule (or, for that matter, can pertain to the liquid or solid state) with little loss in accuracy (as these constants rarely change by more than 1%, whereas the sign and magnitude of $\Delta\nu$ typically vary from -10 cm^{-1} to $+10$ cm^{-1}, and in some cases much more).[9]

III. The Perturbed Hard Fluid Model and Its Generalization

The PHF model is derived from liquid perturbation theory[27,28] and is used to model the effects of solvation on molecular potential energy surfaces and chemical processes. Briefly, the PHF model treats a liquid as a repulsive reference fluid with a van der Waals mean field representing long-range attractive solute−solvent interactions. The reference system is modeled as a hard-sphere fluid containing a diatomic solute, with diameters realistically representing the solvent of interest, and the solvent density is taken to be that of the pure solvent at the experimental temperature and pressure. In previous PHF studies, attractive solute−solvent interactions have been assumed to have a linear density dependence (in keeping with the van der Waals mean-field approximation). In the present work, this approximation is relaxed in order to better represent short-range attractive solute−solvent coupling mechanisms, such as hydrogen bonding. In particular, although attractive interactions were previously represented by a mean-field parameter, the G-PHF model introduces an additional parameter representing the effective length scale of attractive interactions (as described in the Appendix).

When applied to vibrational frequency shifts the G-PHF model predicts that the solvent-induced mean force, F, and the corresponding Δr are determined by a balance of opposing repulsive and attractive contributions.[25] If *repulsive* intermolecular interactions dominate, then $F > 0$, and the solute molecule bond is predicted to *contract* and *blue shift* ($\Delta r < 0$, $\Delta\nu > 0$) with increasing solvent density. In contrast, *attractive* interactions typically contribute a negative force, $F < 0$, and thus a bond length *elongation* and frequency *red shift* ($\Delta r > 0$, $\Delta\nu < 0$).[25] The net change in force, bond length, and frequency can be expressed as the sum of attractive (a) and repulsive (r) contributions.

$$F = F_a + F_r \tag{4}$$

$$\Delta r = \Delta r_a + \Delta r_r \tag{5}$$

$$\Delta\nu = \Delta\nu_a + \Delta\nu_r \tag{6}$$

Although the repulsive and attractive contributions to each of the above equations are usually of opposite sign, this need not always be the case. In particular, although the attractive solvation energy of the excited vibrational state typically exceeds that of the ground state (producing negative values of F_a and $\Delta\nu_a$ and a positive value of Δr_a), in rare cases, it may be that the vibrational excitation produces a decrease in polarizability or dipole moment, and thus, both repulsive and attractive contributions would be positive at all solvent densities (as seems to be the case for the symmetric carbon stretch of acetone).

The repulsive force, F_r, is related in a simple way to the two-cavity distribution function, $y(r)$, in a hard-sphere fluid solvent.[1,5]

$$F_r = -kT\frac{\mathrm{d}\ln[y(r)]}{\mathrm{d}r} \tag{7}$$

Note that $y(r)$ is a function of the solute and solvent diameters and solvent density and that the above derivative with respect to solute bond length is evaluated at the equilibrium bond length (in the ground vibrational state). The required solute and solvent hard-sphere diameters are determined from atomic van der Waals radii and the solvent compressibility data, as described previously.[9]

The van der Waals mean-field approximation implies that the attractive solvation force along the solute bond, F_a, is a linear function of density.[4]

$$F_a = f_a\rho \tag{8}$$

The parameter f_a is a temperature- and density-independent constant. Although predictions based on this approximation (by combining eqs 1, 7, and 8) have been found to agree with high-pressure vibrational frequency shift measurements for a variety of vibrational modes,[1,4,5,8,11,20] C−H and O−H stretch vibrations are notable exceptions[1,8,20] (as explained in section I).

In an attempt to better account for the nonlinear behavior of C−H and O−H stretch vibrations, the G-PHF model includes the following more general expression for F_a (whose derivation is given in the Appendix)

$$F_a = f_a\rho[1 + Rg(\sigma_c)] \tag{9}$$

where f_a can be equated with the van der Waals mean field coefficient, $g(\sigma_c)$ is the value of the solvent radial distribution function at solute contact (see Appendix), and R is a new parameter describing the length scale of attractive interactions. If the solute−solvent cohesive interaction is assumed to drop off as $(1/r)^n$, where r is now the solute−solvent separation, then $R \approx 0$ corresponds to a system with attractive interactions of long range ($4 < n < 6$), while $R > 1$ corresponds to a system with attractive interactions of very short range ($n \gg 6$). The exact quantitative connection between R and n is expected to depend on the detailed structure of the solute vibrational mode but may be approximately represented by the following relation (with an estimated uncertainty of ± 2 in n, see Appendix for details).

$$n \approx 16R + 3 \tag{10}$$

Thus, eqs 9 and 10 offer *a direct link between the attractive length scale and nonlinearity in the density dependence of* F_a.

IV. Experimental Section

The experimental techniques and the microscope-based Raman system used to measure vibrational frequency shifts at high pressure are similar to those used in previous studies.[1,9,20] The excitation source is a 40-mW HeNe laser (Spectra Physics Model 127), focused onto the sample using a microscope objective (Olympus BH-2). The backscattered Raman signal is collected using the same microscope objective and detected using a liquid-nitrogen-cooled CCD (Princeton Instruments LN/CCD 1152E) mounted to a spectrograph (ISA HR320 F/4.2), with an 1800-grooves/mm grating, with an exposure time of 100 s per spectrum.

For high-pressure studies, the acetone and chloroform-*d* solutions (at a concentration between 10 and 30 wt %) were contained within a 700-μm hole in a 500-μm-thick stainless steel gasket in a Merrill−Basset diamond anvil cell (DAC). Measurements were taken at room temperature (23 ± 2 °C) and pressures up to 2.7 GPa in acetone solutions and 3 GPa in chloroform-*d* solutions. Spectral-grade acetone was purchased from Mallinckrodt. Samples of chloroform-*d*, dichloromethane, tetrahydrofuran, and methanol were purchased from Aldrich Chemical Co. All chemicals were used as received.

Pressure-to-density conversions were performed using the Carnahan Starling−van der Waals (CS−vdW) equation of state[2,3] with parameters obtained from the compressibilities of the corresponding pure liquids (as described in ref 20).[2,3]

Infrared frequency shifts for dilute *n*-butanol solutions were obtained from Fishman and Drickamer,[10] who measured O−H stretch frequencies of *n*-butanol monomers in various solvents at pressures up to 1.2 GPa and 25 °C. The high-pressure frequency shifts of N_2, ethane (C−H and C−C), and methyl iodide (C−I) were obtained from previously reported Raman measurements.[8,11,20] Frequency shift results for all solutions used in this paper are collected in Table 1. Frequency shifts relative to the dilute vapor were determined by subtracting peak frequencies in solution from the corresponding gas-phase Q-branch frequencies (with centrifugal correction when needed).[1,29]

The experimental precision of vibrational frequency shift measurements is typically on the order of ± 0.5 cm^{-1}. This experimental uncertainty propagates to produce a precision of about ± 0.3 pm in the change in solute bond length and ± 8 pN in the solvent-induced force along the bond (although the absolute bond length change and force values may be less accurate, as described in section III). All of the pertinent solute and solvent parameters are collected in Tables 1 and 2.

V. Results and Discussion

Figure 1 represents the vibrational frequency shifts of N_2 as a function of density (at $T = 295$ K), including both experi-

TABLE 1: Experimental Frequency Shifts, Forces, and Changes in Bond Length

sample number	solute[a]	solvent	pressure (GPa)	density (molecules/nm^3)	$\Delta\nu$ (cm^{-1}) $\pm$ 0.4	E (pN) $\pm$ 8	Δr (pm) $\pm$ 0.3
1	nitrogen (N_2)	nitrogen (N_2)[b]	0.03	7.0	−1.0	−27	0.01
			0.23	16.1	−1.2	−32	0.01
			1.99	26.4	3.8	101	−0.04
2	C−C, ethane $\rho_0 = 13.02$	ethane[c]	0.0001	6.8	−0.2	−5	0.01
			0.78	14.3	8.7	176	−0.36
			2.56	16.7	22.3	449	−0.92
3	C−C, ethane $\rho_0 = 9.67$	methylene chloride[c]	0.04	9.7	0.6	12	−0.02
			0.81	11.9	6.7	134	−0.28
			2.08	13.1	15.8	318	−0.65
4	C−C, acetone $\rho_0 = 7.40$	tetrahydrofuran	0.19	8.1	8.8	167	−0.38
			1.24	9.4	18.5	353	−0.80
			2.88	10.1	28.3	540	−1.23
5	C−C, acetone $\rho_0 = 9.37$	methylene chloride	0.0001	9.4	5.9	112	−0.25
			0.31	10.9	12.1	230	−0.52
			2.90	13.5	31.8	606	−1.38
6	C−D, chloroform-*d* $\rho_0 = 9.37$	methylene chloride	0.0001	9.4	−8.9	−62	0.13
			0.59	11.5	−8.1	−56	0.11
			0.71	11.7	−8.0	−56	0.11
7	C−D, chloroform-*d* $\rho_0 = 7.40$	tetrahydrofuran	0.0001	7.4	−15.1	−105	0.21
			0.82	9.1	−15.9	−111	0.22
			1.77	9.7	−13.1	−91	0.19
8	C−H, ethane $\rho_0 = 13.02$[d]	ethane[c]	1.03	14.9	−5.5	−29	0.06
			1.97	16.2	1.3	7	−0.01
			2.56	16.7	5.3	28	−0.06
9	C−H, ethane $\rho_0 = 9.67$	methylene chloride[c]	0.05	9.7	−10.8	−57	0.12
			1.00	12.1	−7.7	−41	0.09
			2.08	13.1	0.0	−0.1	0.0002
10	C−Cl, chloroform-*d* $\rho_0 = 9.37$	methylene chloride	0.0001	9.4	−11.1	−231	0.71
			0.59	11.5	−9.6	−201	0.62
			0.71	11.7	−7.1	−149	0.46
11	C−Cl, chloroform-*d* $\rho_0 = 7.40$	tetrahydrofuran	0.0001	7.4	−12.2	−255	0.79
			0.82	9.1	−10.2	−213	0.66
			1.77	9.7	−7.2	−150	0.47
12	C−Cl, chloroform-*d* $\rho_0 = 14.85$	methanol	0.0001	14.8	−10.1	−210	0.65
			1.52	20.7	−6.7	−139	0.43
			3.25	22.6	−1.6	−33	0.10
13	C−I, methyl iodide $\rho_0 = 9.67$	methyl iodide[c]	0.004	9.7	−6.9	−129	0.57
			0.18	10.7	−5.7	−106	0.46
			0.67	11.9	−2.3	−44	0.19
14	O−H, *n*-butanol $\rho_0 = 9.93$	CS_2[e]	0.0001	9.9	−47.6	−303	0.39
			0.58	12.3	−62.6	−398	0.51
			1.13	13.1	−71.6	−456	0.58
15	O−H, *n*-butanol $\rho_0 = 5.64$	toluene[e]	0.0001	5.6	−65.6	−417	0.54
			0.53	6.6	−79.6	−506	0.65
			0.85	6.9	-−87.6	−557	0.71
16	O−H, *n*-butanol $\rho_0 = 6.54$	*n*-propyl bromide[e]	0.0001	6.5	−69.6	−443	0.57
			0.37	7.8	−83.6	−532	0.68
			1.05	8.6	−90.6	−576	0.74
17	O−H, *n*-butanol $\rho_0 = 5.31$	*n*-propyl iodide[e]	0.0001	5.3	−77.6	−494	0.63
			0.58	6.5	−108.6	−691	0.89
			1.16	6.9	−118.6	−754	0.97
18	O−H, *n*-butanol $\rho_0 = 4.63$	2,3-dimethylbutane[e]	0.0001	4.6	−23.6	−150	0.19
			0.32	5.6	−28.6	−182	0.23
			0.95	6.2	−34.6	−220	0.28

[a] Solute vibrational mode and structure are listed above the number density of the solvent at 1 atm, ρ_0, in units of molecules/nm^3. [b] Obtained from refs 11 and 20. [c] Obtained from ref 8. [d] The density, ρ_0, is that of the liquid at the triple point. [e] Obtained from ref 10.

mental measurements (points)[11,20] and G-PHF predictions (curves). This figure clearly shows the good agreement between experimental pressure shifts and G-PHF predictions, as well as the predicted repulsive and attractive frequency shift contributions derived by the generalized PHF analysis. Note that, although the attractive shift was derived from a G-PHF fit to the experimental data (using eqs 7 and 9), the results confirm the nearly linear dependence of the attractive frequency shift (dotted curve in Figure 1). This implies that a relatively long-range attractive coupling mechanism is responsible for the red shift of the N_2 peaks at low densities, in close agreement with van der Waals mean-field predictions (eq 8).

The subpanels in Figure 2 represent the vibrational frequency shifts, solvent-induced force, and the change in bond length of N_2 as a function of solvent density (left-hand panels) or pressure (right-hand panels). Again, the solid curves represent the predictions of the perturbed hard fluid model (fit to the experimental data). These results clearly illustrate the close affinity between $\Delta\nu$, F, and Δr. Except for the opposite sign of Δr (see section II), all of these quantities display a similar characteristic density and pressure dependence. Another interesting feature of these results is the remarkably linear pressure dependence of $\Delta\nu$, F, and Δr at high pressures. This behavior suggests a very simple mechanistic explanation, as the force

TABLE 2: Solute and Solvent Parameters

sample number[j]	υ_0 (cm^{-1})	r_0 (Å)	σ_1 (Å)	σ_2 (Å)	σ_S (Å)	f (N/cm)	A r_0g/f	f_a^i (cm^{-1} nm^3)	R
1	2330[a]	1.10[a]	3.1[a]	3.1[a]	3.45[a]	22.95[a]	−2.71[a]	0.193	0.136
2	994.8[b]	1.54[a]	3.4[a]	3.4[a]	4.23[b]	4.87[a]	−2.50[a]	0.0019	0.0125
3	–	–	–	–	4.63[b]	–	–	0.446	0.000038
4	780[a]	1.51[a]	–	–	5.15[f]	4.40[a]	−2.98[a]	0.221	−0.000175
5	–	–	–	–	4.63[f]	–	–	0.321	0.000412
6	2261.5[c]	1.07[c]	3.4[a]	2.4[a]	4.63[f]	4.93[g]	−2.24[h]	0.536	1.504
7	–	–	–	–	5.15[f]	–	–	0.5780	2.488
8	2953.8[b]	1.10[a]	–	–	4.23[b]	4.74[a]	−2.21[a]	1.01	0.605
9	–	–	–	–	4.63[b]	–	–	0.429	2.704
10	659[c]	1.76[c]	3.4[e]	3.5[e]	3.83[f]	3.23[g]	−2.76[h]	1.58	0.000207
11	–	–	–	–	4.63[f]	–	–	1.850	0.108
12	–	–	–	–	5.15[f]	–	–	0.668	0.272
13	533[b]	2.13[b]	4.1[b]	3.66[b]	4.59[a]	2.28[a]	−3.28[a]	1.254	−0.00860
14	3671.6[d]	0.97[a]	3.04[a]	2.4[a]	4.51[f]	7.80[a]	−2.16[a]	1.79	1.344
15	–	–	–	–	5.72[f]	–	–	6.178	0.621
16	–	–	–	–	5.26[f]	–	–	8.753	0.213
17	–	–	–	–	5.74[f]	–	–	6.660	0.801
18	–	–	–	–	5.92[f]	–	–	1.359	2.223

[a] Obtained from ref 9. [b] Obtained from ref 8. [c] Obtained from ref 34. [d] Measured using FT-IR. [e] Obtained from ref 30. [f] Solvent diameters calculated from the CS-vdW equation of state (ref 2). [g] Obtained from ref 33. [h] Calculated from bond length, bond energy, and harmonic force constant. [i] The units of f_a pertain to attractive frequency shift in cm^{-1} and density in nm^{-3}. [j] See Table 1.

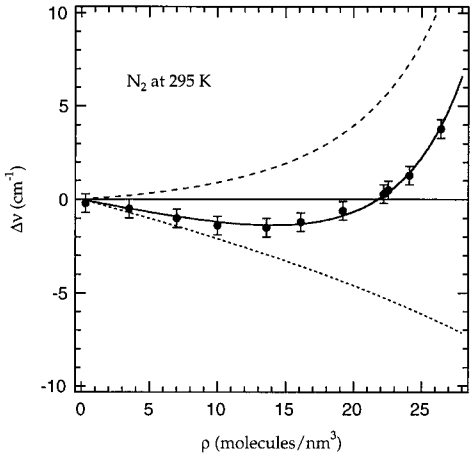

Figure 1. Vibrational frequency shift of N_2 at 295 K. The circles represent the results of previous Raman measurements.[11,20] The three curves are generalized perturbed hard fluid (G-PHF) predictions for the attractive (dotted curve), repulsive (dashed curve), and total (solid curve) frequency shift (obtained from a fit to the experimental points, as described in sections II and III).

along a diatomic bond in a hydrodynamic continuum solvent should be equal to a product of the pressure and the effective cross-sectional area along which the pressure is exerted.[9] Thus, the linear pressure dependence at high pressure suggests that repulsive solute−solvent interactions couple to the N_2 bond with a cross section that is roughly pressure-independent and similar in magnitude to the cross-sectional area of one nitrogen atom (∼8 Å^2). The nonlinear pressure dependence at low pressures reflects the turnover from attraction-dominated to repulsion-dominated solvation over the gas-to-liquid pressure range.

The magnitude of the red shift at low densities (and pressures) depends on the strength of the attractive solute−solvent interactions or, more specifically, on the increase in solvation energy upon excitation from the $\upsilon = 0$ to the $\upsilon = 1$ vibrational state of N_2. Because such attractive interactions are expected to be largely due to dispersion forces, they should scale with the polarizability of the solvent (and the polarizability derivative of the solute).[1] The magnitude of these interactions can be quantified by determining the attractive mean-field parameter, f_a (in eq 7), obtained from high-pressure frequency shifts of N_2 in different solvents.[30] The results reveal a linear dependence

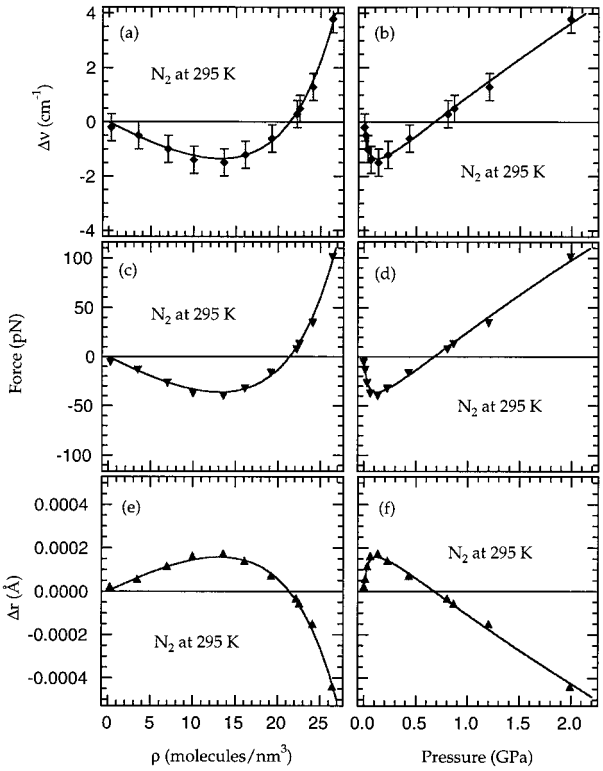

Figure 2. Density and pressure dependence of the frequency shift, $\Delta\nu$, force, F, and change in bond length, Δr, for N_2 at 295 K.

of f_a on solvent polarizability, in solvents ranging from argon to *n*-hexane and methanol. Such results confirm the fundamental soundness of the van der Waals mean-field approximation in describing the attractive solute−solvent interactions in these solutions.

Figure 3 illustrates the density-dependent frequency shift behavior of a wide range of other liquid systems. Each of the four subpanels in this figure contains the experimental frequency shifts for different types of bonds in various fluids (points) and the G-PHF model predictions (curves). The frequency shifts of C−C bonds are positive and become more positive as the pressure increases (blue shift). For C−X (X = F, Br, Cl, and I), C−D, and C−H bonds, a minimum in the frequency shift is

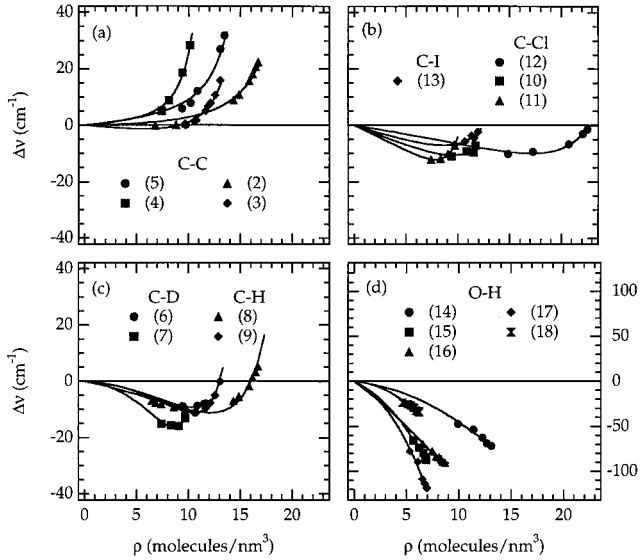

Figure 3. Density dependence of the frequency shift in different solutions. The symbols represent the results of Raman and infrared measurements, and the solid curves are G-PHF predictions (see Table 1 for the solute and solvent molecules corresponding to each number).

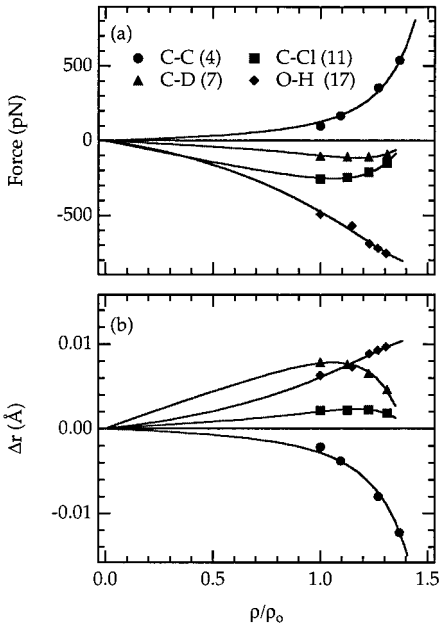

Figure 4. Solute frequency shift results translated into (a) a pressure-induced force and (b) the change in bond lengths for different solute vibrations, plotted as a function of reduced solvent density (see Table 1 for the solute and solvent molecules corresponding to each number).

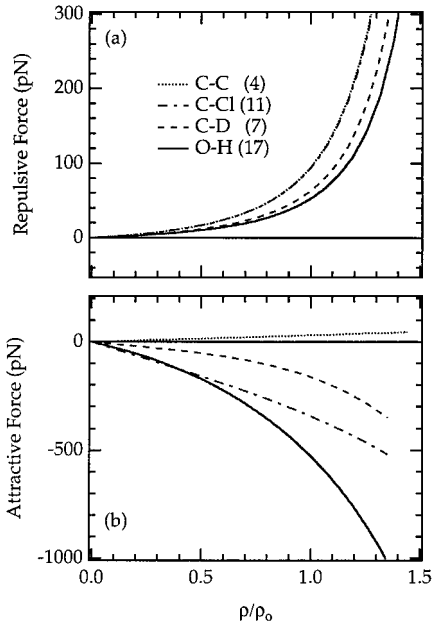

Figure 5. (a) Repulsive and (b) attractive solvation forces along different solute bonds are plotted as a function of reduced solvent density (see Table 1 for the solute and solvent molecules corresponding to each number).

evident (and occurs at densities not far from that of the ambient liquid). The sharp blue shift (with positive curvature) evident at high densities in sub-panels a, b, and c marks the onset of strong repulsive interactions between the solute and solvent. On the other hand, the nonlinear red shift (with negative curvature) of the O−H vibrations suggests the presence of an attractive solute−solvent interaction mechanism that turns on increasingly strongly at high densities. A similar, nonlinear red shift appears to occur for C−H and C−D vibrations at lower densities (although this is more difficult to measure because of the thermodynamic inaccessibility of the vapor−liquid region in these systems and because the attractive shift of C−H and C−D vibrations is smaller in magnitude that of O−H vibrations). Furthermore, studies of supercritical fluid CH_4 and CH_3-CH_3,[11] as well as cyclohexane dissolved in CO_2,[12] indicate that the symmetric C−H stretch vibrations in these systems shift nearly linearly with density up to near critical densities. Thus, the negative curvature of the C−H frequency shifts appears to occur predominantly above critical densities.

Figure 4a shows the solvent-induced force along different bonds as a function of solvent density (relative to the density of the ambient liquid, ρ_0). Figure 4b represents the change in bond length of the corresponding solute bonds as a function of reduced solvent density. The results in Figure 4 mirror those of the associated frequency shifts (shown in Figure 3), although the relative magnitudes of the F_{g-l} and Δr_{g-l} values for different systems depend on the magnitude of the associated vibrational parameters f, g, and ν_e.

Figure 5 shows G-PHF-derived (a) repulsive and (b) attractive contributions to the overall solvation forces calculated using eq 7 and fit to the experimental frequency shifts in each system. Clearly, the magnitude of the solvent-induced repulsive forces is relatively insensitive to solute and solvent parameter differences, although the repulsive forces along the O−H and C−H (or C−D) bonds are slightly smaller than those along bonds between two larger atoms. On the other hand, attractive solvation forces depend much more strongly on solute and solvent parameters. The attractive force along the C−C bonds is very small and apparently nearly perfectly linear (and the acetone C−C stretch is unusual in having a positive sign). This behavior is reminiscent of that for N_2 (see Figure 1) and is characteristic of nonpolar bonds with small polarizability derivatives (low Raman cross sections).[9]

The attractive solvent induced force along C−X (X = F, Br, Cl, and I) bonds is invariably large and negative, in keeping with the larger dipole and polarizability derivative of these bonds. The very slight apparent nonlinearity of the attractive force along carbon−halogen bonds is generally consistent with an attractive interaction length scale proportional to $(1/r)^{5\pm2}$. The attractive force along the C−Cl bond of $CDCl_3$ dissolved in CH_3OH appears to have a somewhat shorter range than the other CCl bonds and may be indicative of a local interaction, such as a CCl···HO hydrogen bond, in this system.

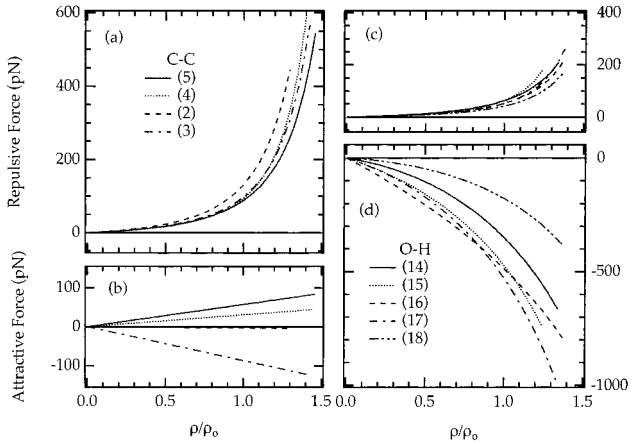

Figure 6. Repulsive and attractive solvation forces along the C−C bond of acetone and ethane in different solvents (a and b, respectively) and the O−H bond of *n*-butanol in different solvents (c and d, respectively) are plotted as a function of reduced solvent density (see Table 1 for the solute and solvent molecules corresponding to each number).

The attractive force derived from hydrogen frequency shifts (C−H, C−D, and O−H stretches) is clearly a strongly nonlinear function of solvent density (Figure 5b, solid and dashed curves). The short-range attractive force parameter derived from these data has an average value of $R \sim 1.38$ (eq 9), which suggests an average attractive length scale of $n \sim 25$ (eq 10). This very large n value is suggests an attractive interaction mechanism with a much shorter length scale than spherically angle averaged dispersive or dipolar interactions.

Figure 6 compares the qualitative and quantitative differences between repulsive and attractive solvent-induced forces along solute C−C and O−H bonds (which represent two extremes in the range of pressure-induced frequency shift behaviors shown in Figure 3). In each case, results in several solute−solvent systems are shown. Figure 6a and b clearly indicates the predominance of repulsive solute−solvent interactions for C−C bonds. In the case of O−H bonds (Figure 6c and d), the opposite is true, as attractive interactions clearly predominate at all densities. This figure again clearly illustrates the characteristically different density dependence of the attractive force along these two bonds (linear for C−C bonds and very nonlinear for O−H bonds).

VI. Conclusions

Solute vibrational frequency shift measurements are used to quantitate intermolecular forces and the resulting changes in solute bond lengths as a function of solvent density (or pressure). The results show marked differences between the forces experienced by different types of bonds. The general trends in the observed behavior can be understood by considering the fundamental mechanisms underlying intermolecular interactions. Because most normal-mode vibrations involve an increase in both polarizability (or dipole moment) and volume upon vibrational excitation, the resulting attractive and repulsive solvation forces are typically opposite in sign.

The G-PHF model appears to contain all of the physical ingredients needed to explain the wide range of the experimentally observed gas-to-liquid and pressure-induced vibrational frequency shifts. The independently determined parameters of this model are the solvent density and temperature and the solute atomic and solvent molecular hard-sphere diameters.[2,3] The only adjustable parameters in the G-PHF model are f_a and R, which describe the magnitude and nonlinearity of the attractive solute−solvent coupling mechanism. The resulting R values can be used to infer the effective attractive length scale, n, assuming a spherically averaged interaction proportional to $-1/r^n$ (see eq 10 and the Appendix).

Both experimental and G-PHF results suggest that repulsive solvation forces at a given pressure are dictated primarily by the size of the vibrating solute atom. Because atomic radii are relatively constant across the periodic table, the resulting repulsive solvation forces are also relatively invariant. Quantitatively, the repulsive cross-sections derived from high-pressure frequency shifts range from 8 to 13 Å^2, implying a diameter of 3−4 Å, in very good agreement with standard atomic van der Waals diameters.[31]

Given the similarity of repulsive solvation forces (at a given pressure), it is clear that the tremendous variation between solvation forces in different systems is largely dictated by the variability in the attractive solute−solvent coupling mechanisms. The G-PHF analysis of N_2, CC, CCl, and CI frequency shifts in various solvents indicates that the attractive mean force responsible for the red gas-to-liquid shifts in these systems typically has a relatively long length scale, with $n \approx 5 \pm 2$. On the other hand, a similar analysis of O−H, C−H, and C−D frequency shifts suggests the presence of a much shorter-ranged cohesive interaction, with $n \approx 25 \pm 10$.

Although the value of n alone cannot be used to uniquely determine the underlying solute−solvent coupling mechanism, the large n values derived from hydrogen frequency shifts are suggestive of hydrogen-bond formation. Given the well-known propensity of O−H groups to form hydrogen bonds, perhaps the most surprising aspect of these results is not the existence of such short length scale interactions but their ubiquity. In particular, not only O−H in polar solvents but also O−H in nonpolar solvents (i.e., butanol monomers in CS_2 and 2,4-dimethylpentane) appears to form short-range intermolecular bonds at high pressure. Similarly, C−H and C−D frequency shifts reveal the presence of a comparably short solute−solvent cohesive coupling mechanism, although the interaction is most evident in polar solvents and its magnitude is generally not as great as that for O−H groups.[8]

Taken together, these results suggest a universal propensity for hydrogen atoms to form very short-ranged cohesive interactions with other molecules. The ubiquity of this behavior appears to require a more general definition of hydrogen bonding or the identification of an alternative short-range cohesive coupling mechanism available only to hydrogen (and deuterium) atoms. For example, it is possible that the short range of the solute−solvent interaction of hydrogen vibrations derives from the small size and mass of a hydrogen atom, rather than from true hydrogen-bond formation. In other words, localization of the hydrogen vibrational motion may restrict the effective solute−solvent length scale. Perhaps such a geometric effect could contribute to the short range of C−H and O−H vibrations, whereas hydrogen-bond formation may increase the magnitude of the interaction. Thus, the larger frequency shift and force values observed for O−H vibrations (see Figures 3d and 4a) may be the mark of true hydrogen bonding, whereas the short range of C−H interactions may be purely geometric.

Acknowledgment. This work was supported by the National Science Foundation (CHE-9530595).

Appendix: Length Scale Dependence of Attractive Solvation Forces

The van der Waals mean-field approximation is only expected to be appropriate in describing attractive interactions of long

length scale, as it is derived by neglecting short-range correlations in the radial distribution function of the solvent about the solute [i.e., assuming $g(r) \approx 1$].[27,28] On the other hand, if attractive interactions are assumed to have an infinitely short range, then they can be represented by a delta function (or "velcro" potential) that turns on abruptly at solute−solvent contact. In this limit, the solvation force is expected to depend on short-range structural (packing) correlations and so may well not be a linear function of solvent density.

These ideas can be made more quantitative by considering a very simple spherical model for attractive solvation forces, assuming a solute−solvent interaction potential of the following form.

$$u_a = -\epsilon(Q)\left(\frac{\sigma_c}{r}\right)^n = \epsilon_o(Q)(3-n)\left(\frac{\sigma_c}{r}\right)^n \qquad (11)$$

The attractive well depth, ϵ, is assumed to depend linearly on the solute normal-mode coordinate (for small displacements about equilibrium) and σ_c is the contact separation between the solute and solvent (equal to the average of the solute, σ_0, and solvent, σ_s, diameters). The parameter ϵ_0 is a measure of the integrated energy of the attractive interaction in the high-temperature/low-density limit, which is independent of the value of n (for $n > 3$). The solvent configuration-averaged attractive force along the solute normal-mode coordinate can thus be approximately expressed in terms of the following integral over the solute−solvent radial distribution function of the hard-sphere reference fluid, $g(r_r)$, where $r_r = r/\sigma_c$, $d = \sigma_0/\sigma_s$, and the sign convention for F_a is chosen so that a compressive force has a positive sign.

$$F_a = \left[\frac{\pi}{2}\left(\frac{\partial\epsilon}{\partial Q}\right)_e (1+d)^3\sigma_s^3\int_1^\infty g(r_r) r_r^{2-n}\, dr_r\right]\rho \qquad (12)$$

The above expression can be very simply evaluated in the van der Waals mean-field and velcro potential limits. For long-range attractive interactions, the following expression is obtained for the solvent configuration-averaged attractive force along the solute normal mode.

$$F_a \cong \frac{\pi}{2}\left(\frac{\partial\epsilon_o}{\partial Q}\right)_e (1+d)^3\sigma_s^3\rho \propto \rho \qquad (13)$$

On the other hand, in the velcro potential limit, the radial distribution function appearing inside the integral in eq 12 can be replaced by its value at contact, $g(\sigma_c) \equiv g(r_r{=}1)$, leading to the following expression for the force.

$$F_a \cong \frac{\pi}{2}\left(\frac{\partial\epsilon_o}{\partial Q}\right)_e (1+d)^3\sigma_s^3\rho \propto g(\sigma_c)\rho \qquad (14)$$

Note that eq 13, which predicts that F_a should be a linear function of density, is expected to be appropriate for all $n > 3$ in the high-temperature/low-density limit or at arbitrary density in systems with long-range attractive potentials ($n < 6$), because, in both these limits, $g(r) = 1$ is a very good approximation. On the other hand, eq 14, which should be appropriate for an interaction of short length scale ($n \gg 6$), predicts a nonlinear density dependence, because $g(\sigma_c)$ is itself a function of solvent density. The actual density dependence of F_a for intermediate values of n is expected to fall between the limiting behaviors expressed in eqs 13 and 14.

Numerical evaluation of eq 12 for intermediate values of n can be obtained using previous tabulations of the required integrals[7,32] or using the hard fluid (HF) approximation for the solvent radial distribution function[1,5] around a hard-sphere solute of diameter σ_0 dissolved in a hard-sphere fluid of diameter σ_s and density ρ [and assuming $g(r) = 1$ beyond the second solvation shell or after it crosses 1 for the second time].[6] Virtually identical results are obtained by both methods and are indicated by the points in Figure 7. These results pertain to systems with the same solute and solvent diameters but attractive interactions of various length scales and are normalized so as to have the same slope at zero density. The linear and nonlinear dashed curves represent the van der Waals mean-field and velcro limiting behaviors predicted by eqs 13 and 14, respectively. The solid curves represent a fit of these results to eq 9, which assumes that the dependence of F_a on density can be represented by a linear combination of the two limiting results.

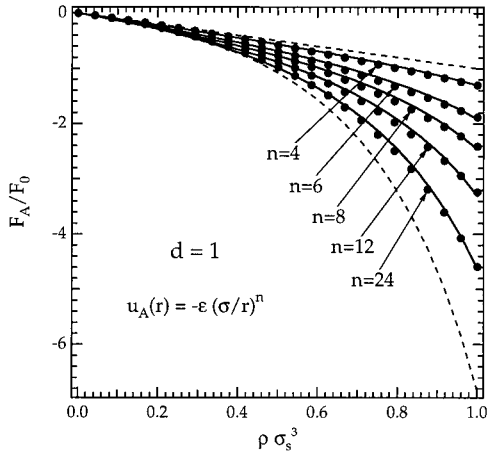

Figure 7. Predicted attractive solvation force (normalized to the same slope at zero density) as a function of reduced solvent density. The attractive interaction can be predicted by varying the values of n in the potential. Points represent results obtained using eq 12, and solid curves represent a fit to eq 9 (with $R = 2.142$, 0.590, 0.293, and 0.169 for $n = 24$, 12, 8, and 6, respectively). The linear and nonlinear dashed curves represent van der Waals mean-field and velcro potential limits, respectively.

Although eq 9 is approximate, the fits shown in Figure 7 clearly indicate that it can be used to reasonably accurately represent the numerical results of eq 12. The parameter R in eq 9 reflects the length scale of the attractive potential, as $R = 0$ for long-range interactions and $R = \infty$ for infinitely short-range interactions. The magnitudes of the two parameters f_a and R should, in general, depend not only on n, but also on the solute−solvent diameter ratio, d. Other calculations performed with a range of diameter ratios ($0.5 \le d \le 1.5$) suggest that eq 10 can be used to approximately relate n to R, with an uncertainty in n of ± 2.

Finally, the above results treat a molecular solute as a sphere with an attractive solute−solvent interaction of an inverse power law form and a well depth that depends linearly on Q (whereas the solute diameter is assumed to be Q-independent), much as has been done in a recent semiclassical analysis of vibrational frequency shifts in supercritical fluids.[16] Although such a spherical approximation is obviously a simplification, it should more or less realistically represent the spherically averaged attractive interactions between nonspherical molecules.

References and Notes

(1) Ben-Amotz, D.; Lee, M.-R.; Cho, S. Y.; List, D. J. *J. Chem. Phys.* **1992**, *96*, 8781.
(2) Ben-Amotz, D.; Willis, K. G. *J. Phys. Chem.* **1993**, *97*, 7736.
(3) Ben-Amotz, D.; Herschbach, D. R. *J. Phys. Chem.* **1990**, *94*, 1038.
(4) Schweizer, K. S.; Chandler, D. *J. Chem. Phys.* **1982**, *76*, 2296.
(5) Ben-Amotz, D.; Herschbach, D. R. *J. Phys. Chem.* **1993**, *97*, 2295.

(6) de Souza, L. E. S.; Ben-Amotz, D. *Mol. Phys.* **1992**, *78*, 137.
(7) Zakin, M. R.; Herschbach, D. R. *J. Chem. Phys.* **1988**, *89*, 2380.
(8) Lee, M.-R.; Ben-Amotz, D. *J. Chem. Phys.* **1993**, *99*, 10074.
(9) Hutchinson, E. J.; Ben-Amotz, D. *J. Phys. Chem. B* **1998**, *102*, 3354.
(10) Fishman, E.; Drickamer, H. G. *J. Chem. Phys.* **1956**, *24*, 548.
(11) Ben-Amotz, D.; LaPlant, F.; Shea, D.; Gardecki, J.; List, D. *American Chemical Society Symposium Series 488*; American Chemical Society: Washington, D.C., 1992.
(12) Pan, X.; McDonald, J. C.; MacPhail, R. A. *J. Chem. Phys.* **1999**, *110*, 1677. Remar, G. J.; MacPhail, R. A. *J. Chem. Phys.* **1995**, *103*, 4381.
(13) de Souza, L. E. S.; Ben-Amotz, D. *J. Chem. Phys.* **1996**, *104*, 139.
(14) Devendorf, G. S.; Ben-Amotz, D.; de Souza, L. E. S. *J. Chem. Phys.* **1996**, *104*, 3479.
(15) de Souza, L. E. S.; Guerin, C. L.; Ben-Amotz, D.; Szleifer, I. *J. Chem. Phys*. **1993**, *99*, 9954.
(16) Egorov, S. A.; Skinner, J. L. *J. Phys. Chem. A* **2000**, *104*, 483.
(17) Pratt, L. R.; Chandler, D. *J. Chem. Phys.* **1980**, *72*, 4045.
(18) Herman, M. F.; Berne, B. J. *Chem. Phys. Lett.* **1981**, *77*, 163.
(19) Herman, M. F.; Berne, B. J. *J. Chem. Phys.* **1983**, *78*, 4103.
(20) Devendorf, G. S.; Ben-Amotz, D. *J. Phys. Chem.* **1993**, *97*, 2307.
(21) Devendorf, G. S.; Hu, M.-H. A.; Ben-Amotz, D. *J. Phys. Chem. A* **1998**, *102*, 10614.
(22) Buckingham, A. D. *Proc. R. Soc. A* **1958**, *248*, 169.
(23) Buckingham, A. D. *Proc. R. Soc. A* **1960**, *255*, 32.
(24) LeSar, R. *J. Chem. Phys.* **1987**, *86*, 4138.
(25) Zakin, M. R.; Herschbach, D. R. *J. Chem. Phys.* **1986**, *85*, 2376.
(26) Devendorf, G. S. Department of Chemistry, Middle Tennessee State University, Murfreesboro, TN. Private communication, 2000.
(27) Hansen, J. P.; McDonald, I. R. *Theory of Simple Liquids*, 2nd ed.; Academic Press: New York, 1986.
(28) Hill, T. L. *An Introduction to Statistical Thermodynamics*, Dover ed.; Dover Publications: New York, 1986.
(29) Shimanouchi, T. *Tables of Molecular Vibrational Frequencies*; NSRDS−NBI 39, 1972; Vol. 1.
(30) Ben-Amotz, D.; de Souza, L. E. S. *Reaction Dynamics in Clusters and Condensed Phases*; Jortner, J., Levine, R. D., Pullman, B., Eds.; Kluwer Academic Publishers: Norwell, MA, 1994.
(31) Bondi, A. *J. Phys. Chem.* **1964**, *68*, 441.
(32) Larsen, B.; Rasaiah, J. C.; Stell, G. *Mol. Phys.* **1977**, *33*, 987.
(33) Galasso, V.; de Alti, G.; Costa, G. *Spectrochim. Acta* **1965**, *21*, 669.
(34) Sverdlov, L. M.; Kovner, M. A.; Krainov, E. P. *Vibrational Spectra of Polyatomic Molecules*; John Wiley & Sons: New York, 1974.